

**PARAMETRIC DEPENDENCE IN MODEL EPIDEMICS. II:  
NON-CONTACT RATE RELATED PARAMETERS**

(IN PRESS, *JOURNAL OF BIOLOGICAL DYNAMICS*)

**W. M. Schaffer<sup>1</sup> and T. V. Bronnikova<sup>2</sup>**

Department of Ecology and Evolutionary Biology  
The University of Arizona  
Tucson, AZ 85721

**Keywords:** Bifurcations, Continuation, Epidemiology, Mathematical models, SEIR Equations.

**Mathematical Subject Classification Codes:** 37M05, 37M20, 65P20, 65P30, 92D30.

---

<sup>1</sup> wms@u.arizona.edu

<sup>2</sup> tvb@u.arizona.edu

**Abstract.**

In a previous paper [1], we discussed the bifurcation structure of *SEIR* equations subject to seasonality. There, the focus was on parameters that affect transmission: the mean contact rate,  $\beta_0$ , and the magnitude of seasonality,  $\varepsilon_B$ . Using numerical continuation and brute force simulation, we characterized a global pattern of parametric dependence in terms of subharmonic resonances and period-doublings of the annual cycle. In the present paper, we extend this analysis and consider the effects of varying *non-contact* related parameters: periods of latency, infection and immunity, and rates of mortality and reproduction, which, following the usual practice, are assumed to be equal. The emergence of several new forms of dynamical complexity notwithstanding, the pattern previously reported is preserved. More precisely, the principal effect of varying non-contact related parameters is to displace bifurcation curves in the  $\beta_0$ - $\varepsilon_B$  parameter plane and to expand or contract the regions of resonance and period-doubling they delimit. Implications of this observation with respect to modeling real-world epidemics are considered.

## Introduction.

*SEIR* and *SEIRS* equations categorize host individuals with respect to disease status: **S**usceptible, **E**xposed (but not yet infectious), **I**nfectious and **R**ecovered (and immune) (Figure 1). As such, they are used to model microparasitic infections for which explicit consideration of parasite load [2, 3] can be neglected. When immunity is permanent, as is approximately true for measles, mumps and rubella, the **R**ecovered class is a sink, and the equations are said to be of the *SEIR* type. In the case of transient immunity, the corresponding acronym is *SEIRS*, the final “S” denoting passage of individuals from the **R**ecovered class to the **S**usceptible. Over the years, an enormous literature on these equations has accumulated, both with regard to their mathematical properties [1, 2, 4-25] and their utility as approximate descriptors of real-world epidemics [8, 9, 14-16, 20, 26-43].

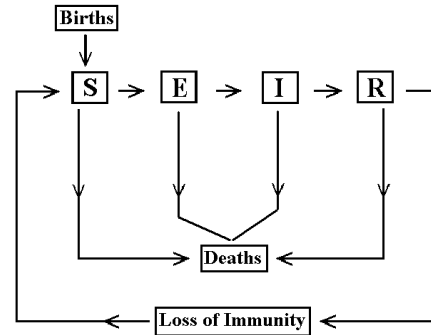


**Figure 1.** *SEIR* and *SEIRS* models of microparasitic infections categorize the host population into four classes. In the absence of vertical transmission, *i.e.*, from mother to fetus, individuals enter the **S**usceptible class at birth, and thereafter progress to the **E**xposed, **I**nfectious and **R**ecovered categories. *SEIR* models presume permanent immunity; *SEIRS* models, transient immunity, with **R**ecovered individuals reverting to the **S**usceptible class.

In the present paper, we focus on the effects of seasonality. Our starting point is a previously described [1] pattern of parametric dependence, the parameters in question being the mean contact rate,  $\beta_0$ , and the magnitude,  $\epsilon_B$ , of seasonal variation thereof. Here, we extend this analysis and consider the consequences of varying *non-contact* related parameters: mortality and reproduction, which, following customary practice, are assumed equal, and periods of latency, infection and immunity. Interestingly, the earlier picture is preserved over a considerable range of parameter values. More precisely, the principal consequences of varying non-contact related parameters are to shift bifurcation curves in one direction or another and to compress or expand the regions they delimit. This suggests an explanation as to why equations that do obvious violence to biological reality can nonetheless be made to harmonize with real-world observations [11, 13, 15, 16]. Specifically, one imagines that the pattern of parametric dependence here described generalizes to more realistic models.

### Preliminaries.

The boxes and arrows in Figure 1 can be implemented in various ways. As in [1], we work with ordinary differential equations, *i.e.*, we ignore the complexities of age structure, spatial extensiveness, explicit time delays and stochastic forcing. We further assume *constant* population size, *quadratic* transmission and *linear* transition between the remaining categories.

Translating these assumptions into mathematics yields

$$\begin{aligned} \frac{dS}{dt} &= m(N - S) - B(t)SI + rR; & \frac{dE}{dt} &= B(t)SI - (m + a)E \\ \frac{dI}{dt} &= aE - (m + g)I; & \frac{dR}{dt} &= gE - (m + r)R \end{aligned} \tag{1a}$$

where  $m^{-1}$  is mean host longevity and  $a^{-1}$ ,  $g^{-1}$  and  $r^{-1}$  are respectively mean periods of latency, infection and immunity. Note the assumption of *seasonal variation* in transmission – the so-called "school year effect" [44] – which we model as a simple trigonometric function, specifically

$$B(t) = B_0(1 + \varepsilon_B \cos 2\pi t). \tag{1b}$$

Here,  $B_0$  is the average contact rate, and  $\varepsilon_B$ , a measure of seasonality.

Because the total population is assumed constant, we substitute  $N - (S + E + I)$  for  $R$  and dispense with the final equation for  $dR/dt$ . This yields

$$\begin{aligned} \frac{dS}{dt} &= (m + r)(N - S) - B(t)SI - r(E + I) \\ \frac{dE}{dt} &= B(t)SI - (m + a)E; & \frac{dI}{dt} &= aE - (m + g)I \end{aligned} \tag{1c}$$

We also replace the remaining state variables with fractions of the total population. That is, we define new variables and parameters,

$$\begin{aligned} s &= S / N; & e &= E / N \\ i &= I / N; & \beta_0 &= B_0 N \end{aligned} \tag{2}$$

This allows us to write

$$\begin{aligned} \frac{ds}{dt} &= (m+r)(1-s) - \beta(t)si - r(e+i) \\ \frac{de}{dt} &= \beta(t)si - (m+a)e; \quad \frac{di}{dt} = ae - (m+g)i \end{aligned} \tag{3a}$$

where

$$\beta(t) = \beta_0(1 + \varepsilon_B \cos 2\pi t). \tag{3b}$$

Equations (3a) are “semi-dimensionless,” having units of inverse time, which we measure in years.

## Methods.

Results were obtained by numerical integration of differential equations and by continuation of periodic itineraries and bifurcation points of Poincaré maps constructed therefrom [1]. The latter were obtained by sampling solution curves of log-transformed versions of Eqs (3) at time intervals equal to the period of forcing, which was one year. Following Schwartz and his associates [26, 27, 42, 43], non-contact related parameters were initially set to  $a = 100 \text{ y}^{-1}$ ;  $g = 35.84 \text{ y}^{-1}$ ,  $m = .02 \text{ y}^{-1}$ ,  $r = 0 \text{ y}^{-1}$ , while  $\beta_0$  and  $\varepsilon_B$  were varied on  $[0, 3000 \text{ y}^{-1}]$  and  $[0, 1]$ . Thereafter, the consequences of varying  $a$  on  $[15, 75 \text{ y}^{-1}]$ ,  $g$  on  $[50, 200 \text{ y}^{-1}]$ ,  $m$  on  $[.01, .04 \text{ y}^{-1}]$  and  $r$  on  $[0, .10 \text{ y}^{-1}]$  were assessed.

Periodic orbits were continued – typically against  $\varepsilon_B$  (Figures 4 and 5) – as described in [1]. Saddle-node and period-doubling bifurcations were identified by application of standard criteria [45, 46]. Continuation of the bifurcations in the  $\beta_0\text{-}\varepsilon_B$  plane yielded the curves shown in Figures 2, 3, 7, 8 and 9. By way of contrast, curves of boundary and interior crises (Figure 2) were identified by brute force inspection [1] of forward and backward bifurcation diagrams.

Resonances were identified by their rotation numbers,  $\rho = m/n$ , where  $n$  is the number of points on a cycle and  $m$ , the number of  $2\pi$  radian rotations required to visit all of them. Strictly speaking,  $\rho$  is only defined for planar mappings, whereas Poincaré maps of Equations (3) are three-dimensional. To first approximation, however,  $E(t)$  and  $I(t)$  are linearly related, *i.e.*,

$$I(t) = \frac{m}{a+g} E(t) + O(\varepsilon) \quad (4)$$

[43]. This justifies approximating the stroboscopic dynamics of Equations (3) as planar maps and the application of two-dimensional constructs, such as rotation number, thereto.

### Autonomous Dynamics.

In the absence of seasonality, *i.e.*, when  $\varepsilon_B = 0$ , Equations (3) manifest equilibril dynamics. More precisely, there are two equilibria. The first is the “no-disease” state,

$$\mathbf{x}^0 = (s^0, e^0, i^0) = (1, 0, 0); \quad (5)$$

the second, the *endemic* state,  $\mathbf{x}^* = (s^*, e^*, i^*)$ , which is given by

$$\begin{aligned} s^* &= R_0^{-1} \\ e^* &= \frac{(m+g)(m+r)}{(m+g)(m+a) + r(m+g+a)} (1 - R_0^{-1}). \\ i^* &= \frac{a(m+r)}{(m+g)(m+a) + r(m+g+a)} (1 - R_0^{-1}) \end{aligned} \quad (6)$$

Here

$$R_0 = \frac{a\beta_0}{(m+a)(m+g)} \quad (7a)$$

is the *basic reproductive rate* of the disease [9, 47, 48], essentially the number of secondary infections that result from a single contagion. For the parameter values considered here,  $a \gg m$  and  $g \gg m$ , from which follows the approximation,

$$R_0 \approx \frac{\beta_0}{g} \quad (7b)$$

From (6), it is obvious that positivity of the endemic state,  $\mathbf{x}^*$ , requires  $R_0 > 1$ . In the case of permanent immunity, *i.e.*, with  $r = 0$ , it can further be shown [30, 33] that  $R_0 > 1$  guarantees that  $x^*$  is *globally stable* on

$$\Omega = \{(s, e, i) \in \mathbf{R}^3 \mid s, e, i \geq 0; s + e + i \leq 1\}. \quad (8)$$

Correspondingly, with  $R_0 < 1$ , it is the no-disease equilibrium that is globally stable.<sup>3</sup> This result is widely believed to hold for the case of transient immunity, *i.e.*, when  $r > 0$ , as well [30], but to date has only been proved in the case that  $r$  is very large or very small [50]. Conversely, with the **R**ecovered class divided into subclasses that delay the return of individuals to the pool of **S**usceptibles, equilibrium dynamics can give way to oscillations [51].

### Non-Autonomous Dynamics.

In the presence of seasonality, the dynamical picture is more complicated. Following [1], we distinguish *modulations of the annual cycle* [26] from *subharmonic resonances* [28, 43]. Viewed in the time domain, the two types of motion are distinct. Subharmonic resonance involves large amplitude cycling, with the number of infectives peaking  $m$  times during the course of an  $n$ -year oscillation with rotation number,  $\rho = m/n$ . By way of contrast, modulations of the annual cycle manifest yearly peaks of smaller magnitude.

Schwartz and Smith [43] were the first to point out that these two dynamical regimes can coexist, in which case there obtain multiple bifurcation sequences – the *main period-doubling* sequence (MPD) of the annual cycle and one or more coexisting subharmonic resonances (CSRs). Alternatively [1], the various motions can be part of a single sequence, in which case there is *unique parametric dependence*. Transition from one case to the other involves sequential incorporation of CSR attractors into the MPD. As discussed in [1], the process is a step-wise affair, proceeding resonance by resonance. Moreover, for each resonance, it is almost always true, *i.e.*, with probability 1, that sequence merging requires the system be “tuned” over an open set of parameter values.

### The $\beta_0$ - $\varepsilon_B$ Control Diagram.

One way of visualizing parametric dependence is via *control diagrams* [31, 45, 46, 52], wherein bifurcations are continued in parameter space. The resulting curves

---

<sup>3</sup> This result is an extension of the theorem first published by [49] for multi-compartment (*e.g.*, males and females) *SI* models. For a wide-ranging review of autonomous models in epidemiology emphasizing the extendibility of this theorem, see [48].

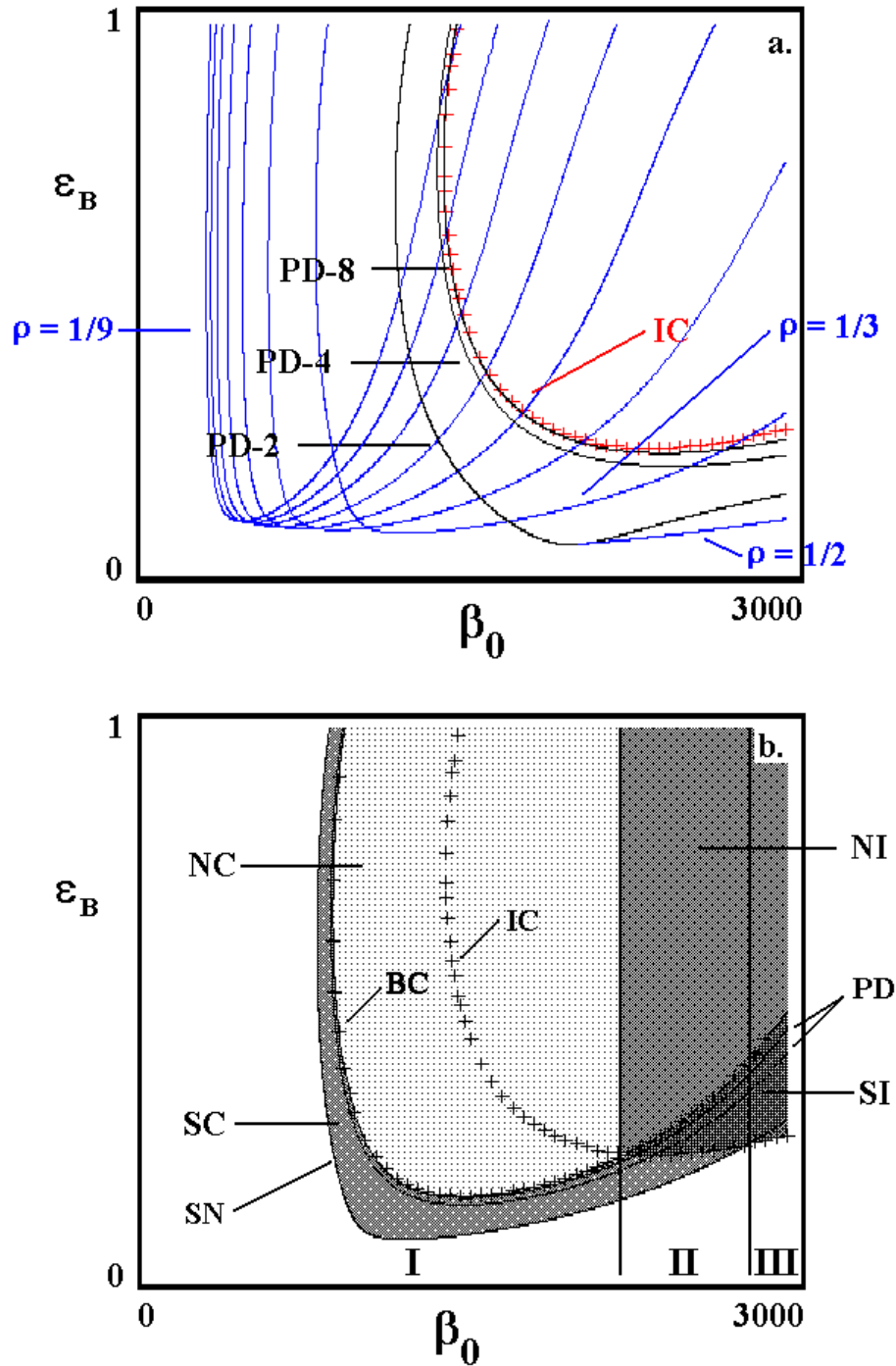


**Figure 2.** The  $\beta_0$ - $\epsilon_B$  control diagram. **a.** Curves of saddle-node bifurcation – identified by rotation number,  $\rho = 1/2$ , *etc.* – are shown in blue; period-doublings of the annual cycle, in black. Red crosses denote interior crises whereby subharmonic resonances are incorporated into the main period-doubling sequence. Here,  $m = 0.02 \text{ y}^{-1}$ ,  $a = 35.84 \text{ y}^{-1}$ ,  $g = 100 \text{ y}^{-1}$  and  $r = 0$ . **b.** The  $\rho = 1/3$  resonance horn showing curves of saddle-node bifurcations (SN), period-doublings (PD) of the nodal cycle and boundary crises (BC) whereby period-3 attractors are destabilized. Differential shading indicates resonance stability and incorporation status vis-à-vis the MPD. NC – non-stable and coexisting; SC – stable and coexisting; NI – non-stable and incorporated; SI – stable and incorporated. As discussed by [1], NC resonances are part of larger chaotic saddles that coexist with MPD attractors. Conversely, SI resonances, when stable, constitute periodic windows on the MPD. Modified from [1].

(surfaces in three dimensions; hypersurfaces in four; ...) divide the diagram into regions corresponding to different dynamical regimes. Overlap of these regions is a necessary, but not a sufficient, condition for coexisting attractors and alternative asymptotic behavior.

Figure 2a displays the  $\beta_0\text{-}\varepsilon_B$  control diagram for Equations (3) for the default parameters:  $a = 100 \text{ y}^{-1}$ ;  $g = 35.84 \text{ y}^{-1}$ ,  $m = .02 \text{ y}^{-1}$  and  $r = 0 \text{ y}^{-1}$ . Two sets of curves are plotted. The blue curves are *saddle-node* bifurcations (SN) that give rise to CSRs; the black curves, *period-doublings* (PD) on the MPD. Also shown is a curve of *interior crises* (IC) at which point MPD dynamics undergo qualitative change [24, 40].

Figure 2b treats the  $\rho = 1/3$  subharmonic in greater detail. Here we identify a curve of  $\rho = 1/3$  saddle-node bifurcations and the first two period-doublings of the stable 3-cycle. Also displayed are a curve of *boundary crises* (BC), whereon period-3 attractors lose stability, and the interior crisis curve of Figure 2a.

Regarding the curves in Figure 2, we remark the following:

1. **Saddle-node Bifurcations.** At each point along a SN curve, two cycles are created or destroyed. Of these, one (the node) is initially stable, but can undergo period-doubling to chaos. The other (the saddle) is initially non-stable and remains so. In Figure 2a, SN curves are labeled according to the rotation number,  $\rho = 1/n$ , ( $n$  is period) of their associated cycles.

2. **Resonance Horns.** Except for the  $\rho = 1/2$  curve (see below), the SN curves delimit regions of parameter space corresponding to cycles of the same base period. These regions are called *resonance horns* – alternatively, *Arnol'd tongues*, after the famous Russian mathematician [53]. Manifestly, the horns pile up at the left, at  $\beta_0 \approx 200$ , a value significantly greater than that ( $\beta_0 \approx g = 35.84$ ) for which the basic reproductive rate,  $R_0 = 1$ . Recalling [43] that Equations (3) are close to a conservative system with  $n$ -periodic solutions that can be excited by seasonality, we imagine the existence of an infinite number of subharmonics, the width of which decreases with increasing period.

Resonance horns typically manifest internal complexity [54], some of which is shown in Figure 2b. Here, we further indicate how CSRs are incorporated into the MPD. As discussed in [1], incorporation begins with BC-IC coincidence (attractor merging [55]), and concludes with IC-SN coincidence (subduction [56]). The coincidences are codimension-2 bifurcations, and generically, they occur at different points in the parameter plane. As a consequence, the control diagram can be divided into three

regions. In region I, all period-3 attractors are off the MPD; in region II, some are incorporated and in region III, all are incorporated. This observation, and the fact that resonant attractors lose stability on the BC curve, leads to a four-way division of the resonance horn: **a.** resonant cycles *stable* and *coexisting* with the MPD (SC); **b.** *non-stable* and coexisting (NC); **c.** stable and *incorporated* (SI) and **d.** non-stable and incorporated (NI).

**3. Period-doubling.** The black curves in Figure 2a correspond to *period-doublings* of the yearly cycle, a process that eventually leads to the emergence of a small amplitude chaotic attractor [26]. As noted above, these motions bear the mark of seasonality, with the number of infectives peaking yearly. Following incorporation of CSRs into the MPD, however, *i.e.*, for parameters above and to the right of the IC curve, this regularity yields to a mix of annual and multi-annual epidemics.

The overlapping nature of the two sets of bifurcation curves makes for a complex choreography in parameter space. Depending on the values of  $\beta_0$  and  $\varepsilon_B$ , subharmonic bifurcation sequences either coexist with or are part of the MPD. In both cases, the resonant cycles can be stable or not. When non-stable, they are part of chaotic sets that themselves may be saddles or attractors [1]. Perhaps surprisingly, all of this can be understood with reference to the curves displayed in Figure 2. From an empirical perspective, the important point is that, even when bifurcation sequences are coexisting, both resonant and the MPD attractors will be visited in the presence of exogenous perturbations and finite population effects [34, 40, 57]. This is consistent with the observation of large amplitude dynamics in small populations for diseases such as chickenpox and measles that manifest low amplitude cycling in large cities [20, 40].

We also note the following sources of additional complexity:

**1. The  $\rho = 1/2$  Bifurcation Curve.** Unlike the other subharmonics, the  $\rho = 1/2$  bifurcation curve does not delimit a horn-like region. Instead, this curve emerges from period-doublings (PD-2) of the annual cycle. Between these two curves, period-2 dynamics coexist with yearly oscillations. Like the BC-IC and IC-SN coincidences noted above, the point at which the  $\rho = 1/2$  resonance originates on PD-2 is a *codimension-2* bifurcation. This point also marks a change in *criticality* of the bifurcations on PD-2. For lower values of  $\beta_0$ , period-doubling is *super-critical*; for higher values, *sub-critical*.

**2. Ultra-Subharmonics.** In addition to subharmonic resonances with rotation number,  $\rho = 1/n$ , there are *ultra-subharmonics* [58], for which

$\rho = m/n$ ,  $m > 1$ . These cycles are also the products of SN bifurcations. They arise in pairs, and the initially stable member period-doubles to chaos [1].

### Response to Varying Non-Contact Rate Related Parameters.

**Loss of Immunity.** The effect of transient immunity, *i.e.*, the transition from *SEIR* to *SEIRS* equations, is shown in Figure 3. Here, the saddle-node and period-doubling bifurcation curves of Figure 2 are recomputed for increasing values of  $r$ . Comparison of the resulting control diagrams with Figure 2a indicates the following:

1. The basic bifurcation structure is preserved, but, with increasing values of  $r$ , the curves are left-shifted, *i.e.*, in the direction of lower values of  $\beta_0$ , and compressed.
2. Relative to the regions of period-doubling, the resonance horns narrow. For sufficiently high values of  $r$ , it is possible that both the horns and the regions of period-doubling disappear entirely. Alternatively, the region of complex dynamics may become so thin as to be effectively unobservable. In either case, rapid loss of immunity promotes annual cycling over dynamical complexity.
3. With increasing values of  $r$  (Figure 3c), a second curve of  $\rho = 1/2$  saddle-node bifurcations emerges from PD-2. Once again, there is a change in criticality - this time from sub- to super-critical. For still larger values of  $r$  (Figure 3e), the saddle-node curves merge. Now there is a closed region of subharmonic period-2 cycles bounded by both saddle-node and period-doubling bifurcations.

Figure 4 explores the consequences to  $\varepsilon_B$  bifurcation diagrams of varying  $\beta_0$  for fixed values of  $r$ . Here, we follow vertical transects in Figure 3d ( $r = .015$ ) for a series of increasing  $\beta_0$  values. Initially (Figure 4a), there is a single supercritical bifurcation that gives rise to a stable period-2 cycle. At this point, period-2 dynamics are modulations of the annual cycle and manifest yearly peaks in incidence. As the transect passes the 1<sup>st</sup> codimension-2 point (origin of the lower SN-2 curve), period-doubling becomes subcritical. (Figure 4b). Now the period-2 cycles are resonant and non-seasonal, *i.e.*, there is one peak every two years. Note that origination of the SN-2 cycles *precedes* the period-doubling bifurcation, *i.e.*, it occurs at a lower value of  $\varepsilon_B$ . Next (Figure 4c), we move our transect past the 2<sup>nd</sup> codimension point (origin of the upper SN-2 curve). Once again, the period-doubling bifurcation changes criticality, and there is a range of  $\varepsilon_B$  values for which resonant and non-

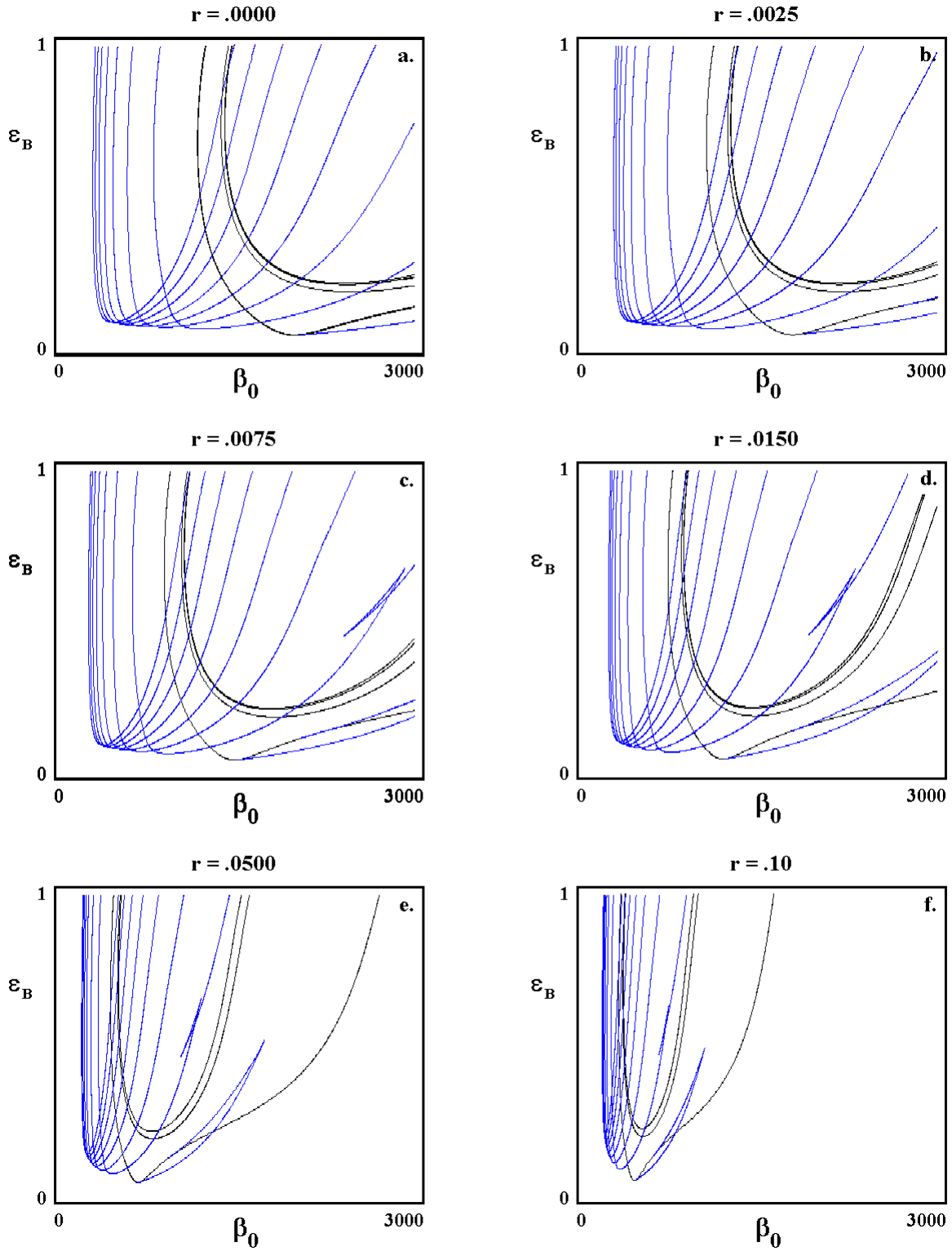


**Figure 3.** Loss of immunity effect. With increasing values of the rate,  $r$ , at which **R**ecovered individuals revert to the **S**usceptible class, the resonance horns are compressed and shifted left. The result is dynamical simplification at high values of  $\beta_0$ . The mean periods of immunity corresponding to the  $r$  values considered are  $\infty$  (permanent immunity), 400, 133, 67, 20 and 10 y. See text for discussion.

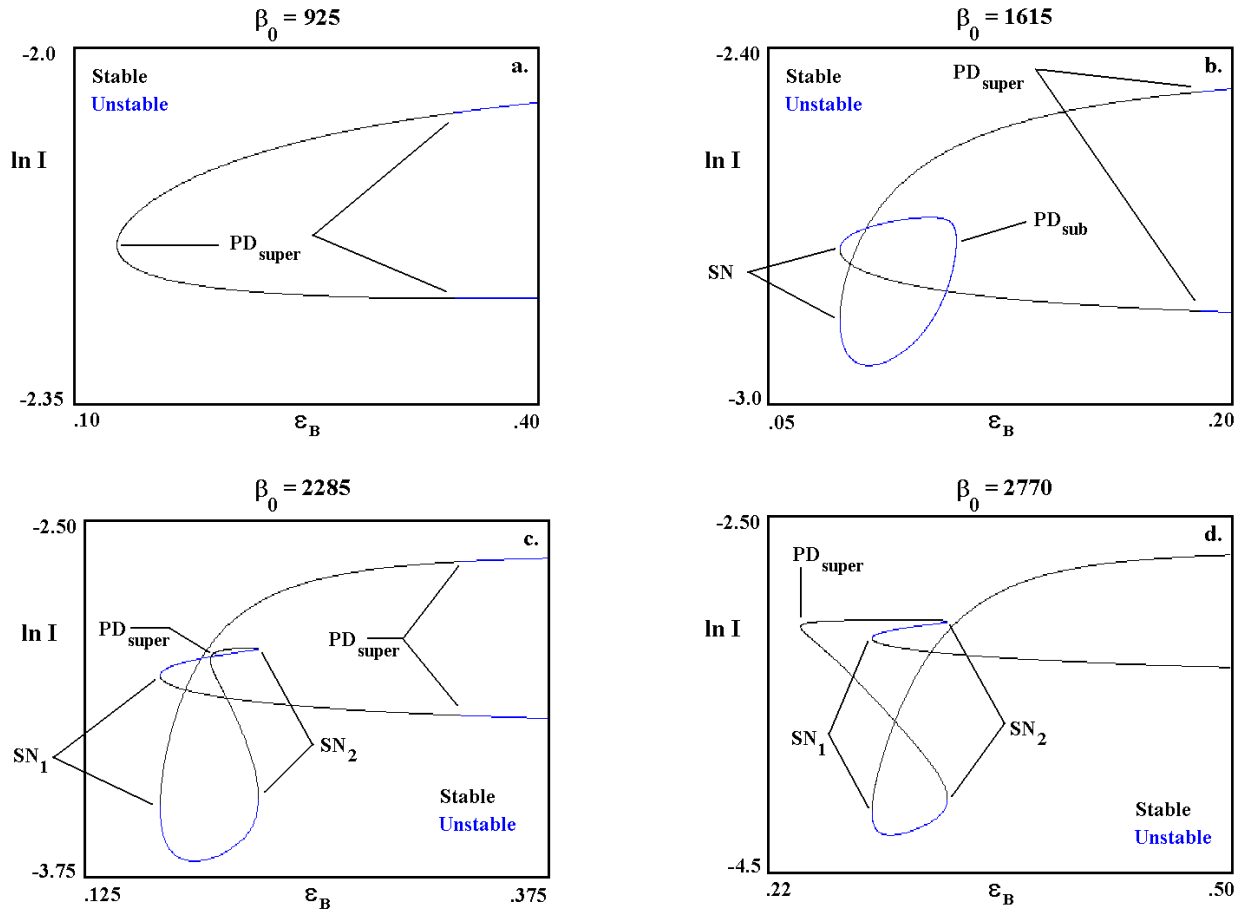


**Figure 4.** Changing period-2 bifurcation diagrams in response to increasing values of  $\beta_0$  for  $r = .015$ . Note changing criticality of period-doubling bifurcations and changing numbers of saddle-node bifurcation. Other parameters as in Figure 2. See text for further discussion.

resonant period-2 cycles coexist (Figures 6a and 6c). Finally (Figure 4d), we place the transect to the right of the point at which the lower SN-2 curve intersects PD-2. Now, it is the MPD cycle that first appears, and, again, there is a range of parameter values for which there are two stable 2-cycles.

In Figure 3d, the two SN-2 curves are distinct – presumably they merge at a value of  $\beta_0$  outside the figure. However, if we jump to Figure 3e ( $r = .05$ ) and follow a transect to the right of the joining point, we are back to the situation in Figure 4a – a single biennial cycle on the MPD.

**4.** The period-3 SN curve also undergoes complication (Figures 3c-3f), with the appearance of a "swallow-tail"-like structure [59]. For parameters within this region there exist a pair of coexisting period-3 cycles (Figure 5). Both have rotation number,  $\rho = 1/3$ , *i.e.*, their Poincaré maps are qualita-

tively the same. However, when plotted in the time domain (Figure 6b) or the  $S$ - $I$  plane (Figure 6d), differences become apparent. One cycle manifests a single peak every three years; the other, two. Because the second cycle peaks twice in one year, the two oscillations are indistinguishable when viewed stroboscopically. The situation is analogous to what one encounters when computing power spectra. With a sampling interval is  $\Delta$ , the highest resolvable frequency is  $(2\Delta)^{-1}$ . Parenthetically, we remark that it is only for periods  $\geq 3$  that  $\rho$  is deducible from the Poincaré map. That is, distinguishing  $\rho = 1/2$  oscillations from doublings of the annual cycle ( $\rho = 2/2$ ) requires knowledge of the time series as well as the map.

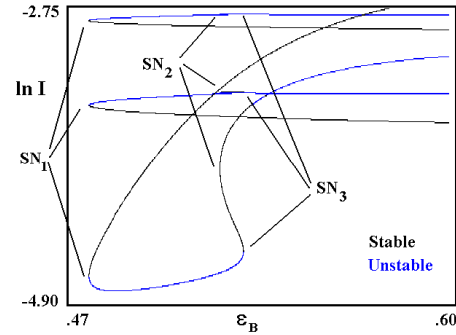


**Figure 5.** With transient immunity, the possibility of multiple period-3 saddle-node bifurcations –  $SN_1$ ,  $SN_2$  and  $SN_3$  – arises. The result is two pairs of period-3 cycles over a narrow range of  $\varepsilon_B$  values, *i.e.*, between  $SN_2$  and  $SN_3$ . Here,  $\beta_0 = 2617$  and  $r = .0075$ , and the remaining parameters are as in Figure 2. Note that the second and third SN bifurcations are only discernable on the lowest cycle branch, *i.e.*, to make them out on the upper branches would require greater magnification.

Loss rates of natural immunity in diseases such as measles, mumps and rubella are hard to come by. Still, waning vaccine-induced immunity [60, 61], as well as the occasional case report [62], may betoken the fact that  $r = 0$  is only approximate. Sensitivity of the  $\beta_0$ - $\varepsilon_B$  control diagram to small departures from permanent immunity further suggests that the assumption may well be improvident. On the other hand, in the absence of widespread vaccination, repeated exposure of nominally immune individuals to their infectious peers may effectively play the role of booster shots [60]. In this case, however, the boxes and arrows of Figure 1 require modification.

**Other Parameters.** Increased reproduction (increasing the common birth-death rate,  $m$  and reduced latency (increasing the rate,  $a$ , at which Exposed individuals become Infectious), induce changes (Figures 7, 8) in the control diagram similar to those occasioned by reducing the period of immunity. That is, bifurcation curves are left-shifted and compressed. Additionally, complexity involving period-2 cycles and swallow-tails is also observed. Conversely, diminished periods of contagion (increasing the rate,  $g$ , at which infectious individuals recover and become immune), expands the bifurcation curves and shifts them to the right (Figure 9).

With regard to varying  $m$ , it is worth remembering that overall correlations between fertility and mortality notwithstanding [63, 64], these rates do not always change in lockstep. As a result, assessing the dynamical consequences of changing

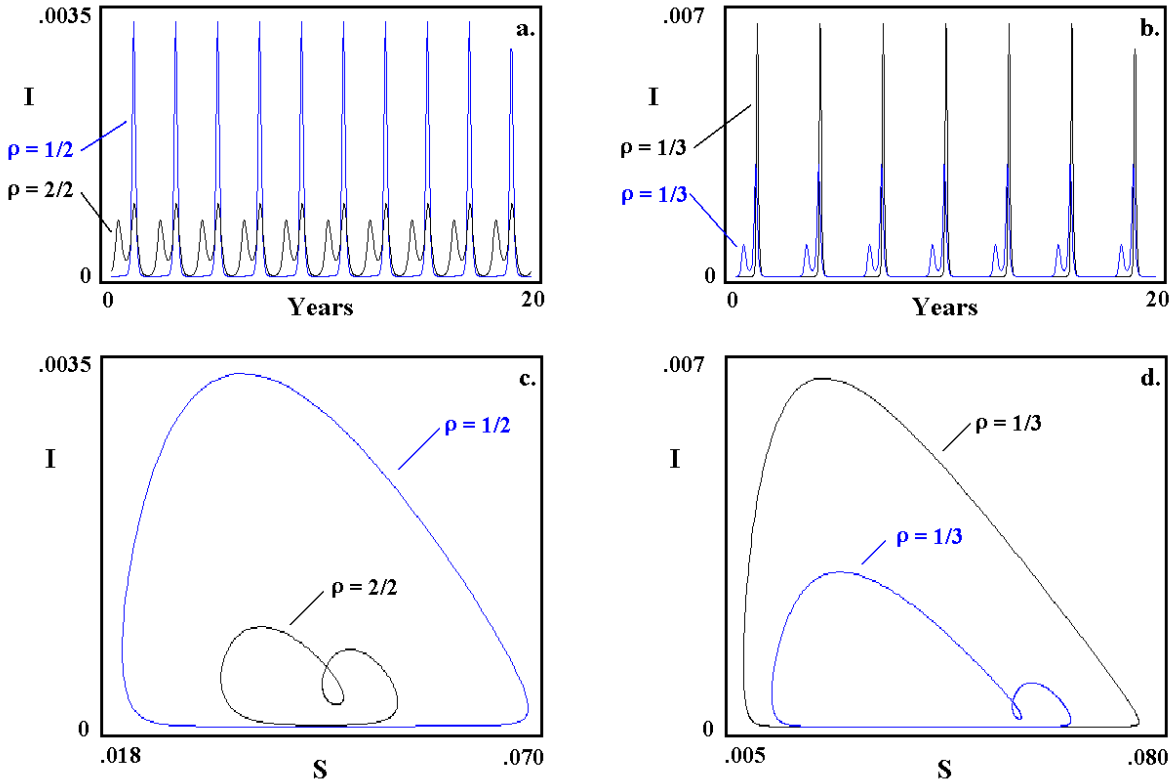


**Figure 6.** Coexisting stable period-2 and period-3 cycles in an *SEIRS* model. **a.** and **c.** Period-2 (biennial) dynamics. Shown in black is a doubling of the annual cycle; shown in blue, a subharmonic resonance. In the former case, incidence peaks every year; in the latter, there is a single peak per oscillation.  $\beta_0 = 2285 \text{ y}^{-1}$ ;  $\varepsilon_B = .203$ ;  $r = .015 \text{ y}^{-1}$ . Other parameters as in Figure 2. **b.** and **d.** Period-3 (triennial) dynamics. Two cycles are observed. Of these, one (shown in black) manifests a single peak in the number of infectives; the other (shown in blue), two peaks. As discussed in the text, these cycles are stroboscopically indistinguishable, *i.e.*, both have  $\rho = 1/3$ , because, in the second case, both peaks occur within a single year.  $\beta_0 = 2617 \text{ y}^{-1}$ ;  $\varepsilon_B = .5241$ ;  $r = .0075 \text{ y}^{-1}$ . Other parameters as in Figure 2.

demography [11] with *any* constant population size model entails unknown, and possibly significant, risks. Pertinent in this regard is the fact that most, if not all, of the time series, *e.g.*, [7, 11, 13, 20, 22, 35, 65, 66], analyzed from the viewpoint of nonlinear dynamics are from populations manifesting substantial changes in number, age structure, life expectancy, *etc.*, during the years in question. For example, many include the years of World War II.

## V. Discussion.

*Tempora mutantur et mutamur.* The results presented here and in [1] sharpen an earlier view [4, 25, 29] of seasonal *SEIR* dynamics, which is that

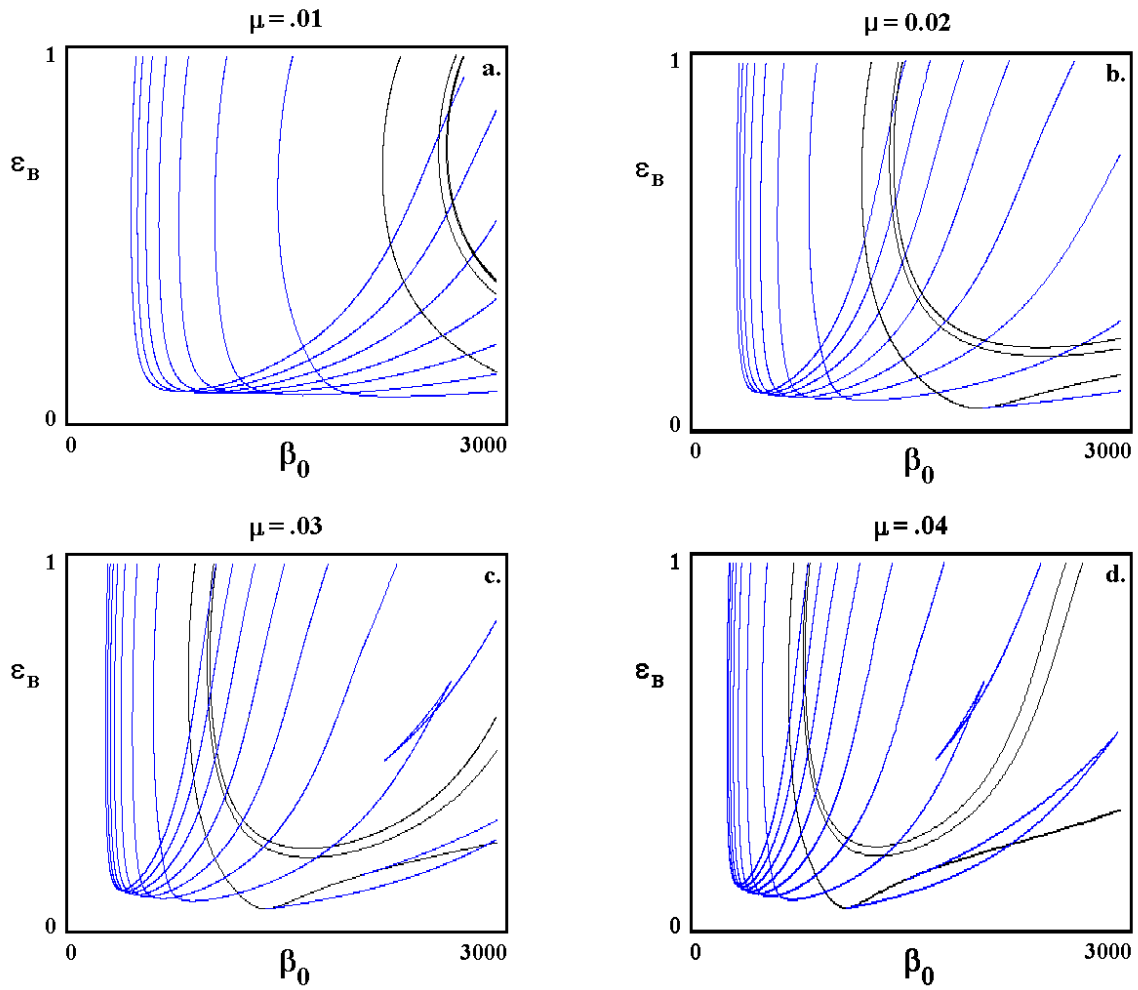


**Figure 7.** Mortality-recruitment effect. With increasing values of  $\mu$  (decreased longevity, increased reproduction) the bifurcation curves are left-shifted and compressed. The values of  $m$  correspond to life expectancies of 100, 50, 33 and 25 y.

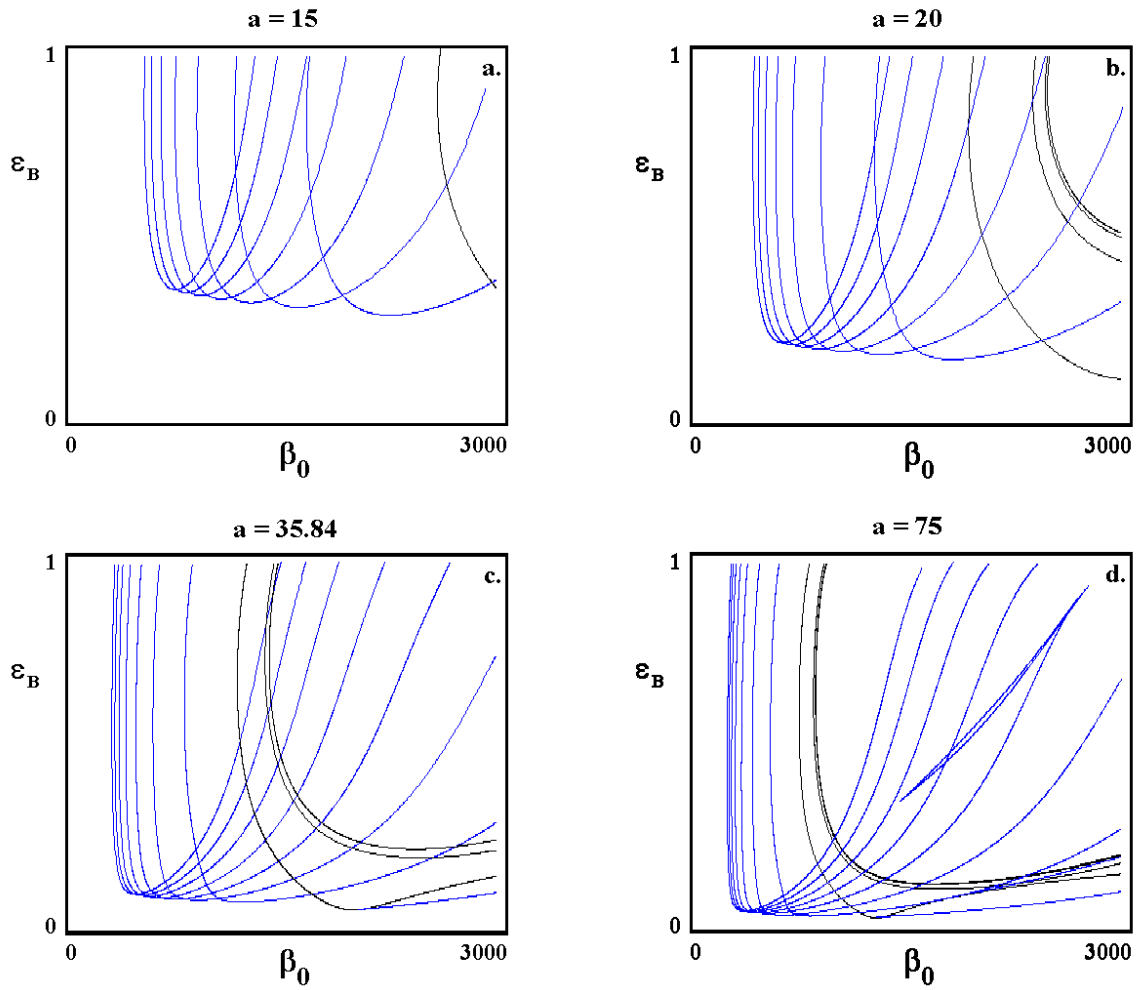


**Figure 8.** Latency effect. With decreasing latency (higher values of  $a$ ), bifurcation curves are left-shifted and the resonance curves compressed. The values of  $a$  correspond to latency periods of 24, 18, 10 and 5 d.

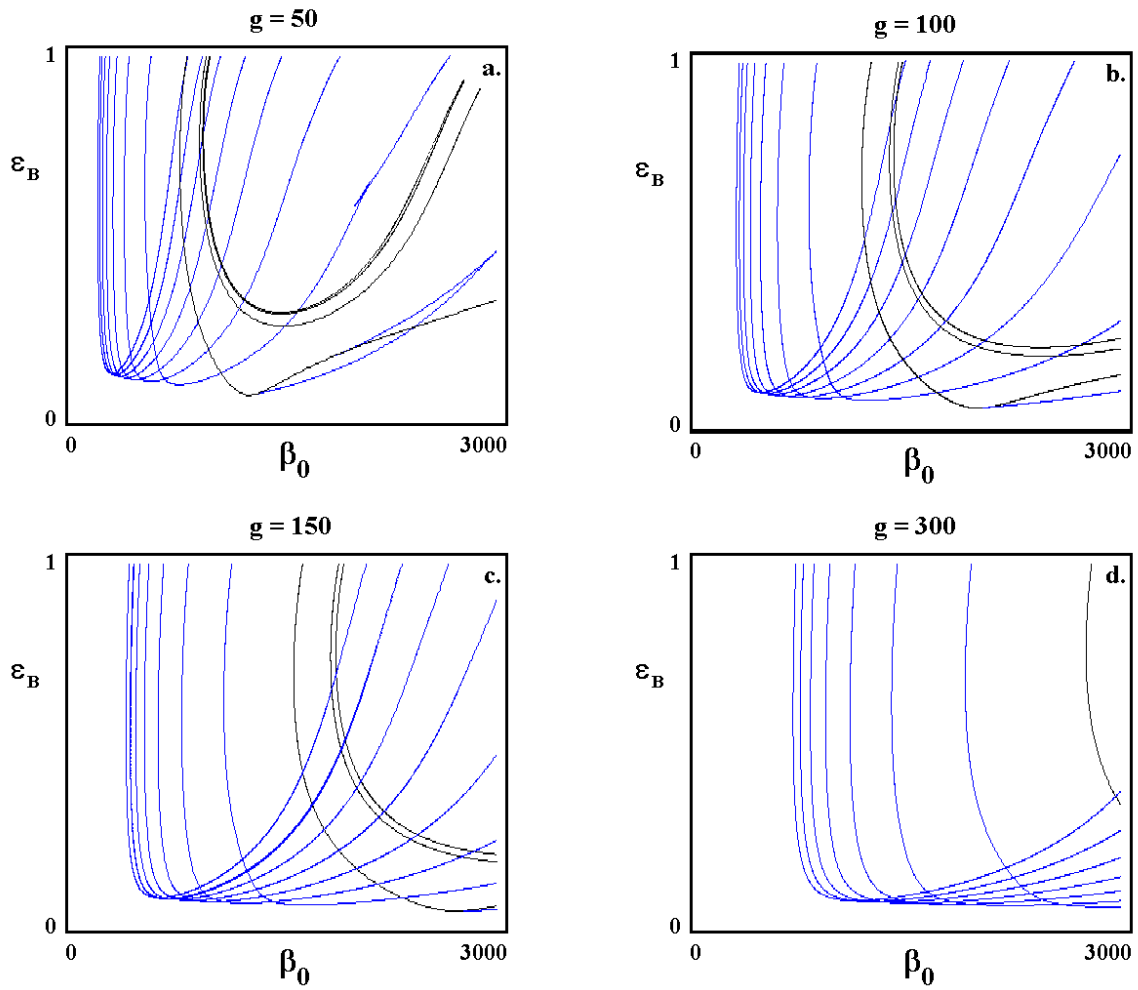


**Figure 9.** Infectious period effect. With decreasing infectious periods (higher values of  $g$ ) bifurcation curves are right-shifted and expanded. The values of  $g$  correspond to infectious periods of 7, 4, 2.4 and 1.2 d.

“seasonal variation in transmission ... can ‘pump’ ... otherwise damped oscillations, locking the system into sustained cycles whose periods are an integral number of years” [47].

We illustrate this state of affairs in Figure 10, wherein saddle-node and period-doubling curves are superposed on the  $\beta_0\text{-}\varepsilon_B$  plane color-coded by  $P$ .<sup>4</sup> Thus,  $P = 1\text{-}2$  y is compatible with resonances of 2-6 y;  $P = 2\text{-}3$  y, with resonances of 2-14 y, *etc.* (Figure 10a). Similarly, all possible values of  $P$  are compatible with annual cycling, while  $P = 1\text{-}3$  y is compatible with all of the period-doublings (Figure 10b).

**Shifting Regions of Complexity.** The pattern of parametric dependence reported here is representative of nonlinear systems subject to periodic forcing [52, 54, 59, 67, 68]. For example, in the course of modeling autonomous kinetics in an enzyme-catalyzed reaction, [69, 70] observed the existence of an oscillatory region outside of which the dynamics are stationary. The corresponding non-autonomous picture [71] is a region of complex periodicity surrounded by period-1 cycles.

An obvious, but nonetheless important, consequence of shifting of regions of complex dynamics involves claims that varying particular parameters is “stabilizing” or “destabilizing.” Often, such assertions require clarification, since the terms only have meaning with regard to the system’s location in parameter space. In the present case, left-shifting the resonance horns can be *destabilizing* for systems to the left of the accumulation point, and *stabilizing* for those to the right of it. In the first instance, one may observe a transition from annual to multi-annual cycles; in the second, multi-annual to annual. With the addition of exogenous perturbations and finite population effects, one expects a mix of behaviors for systems inside the region of complex dynamics and noisy yearly cycling for those outside – see [72].

**An Analogy.** Intuitively, the global dynamical picture makes sense if one analogizes outbreaks of infection to summer wildfires in semi-arid scrub. According to this, **Susceptibles** are the tinder; **Infectives**, the sparks;  $\beta_0$ , the tinder’s flammability, *i.e.*, the per spark likelihood of ignition, and  $\varepsilon_B$ , a measure of the severity of the wet-dry cycle.<sup>5</sup> It follows that there is a minimum combustibility ( $\beta_0 \approx g$ ), below which fires are impossible. Increasing flammability above this value results in annual burns in which only a fraction of the tinder is consumed. With further increases ( $\beta_0 \approx 200$ ), multi-year cycles become possible. Now fuel can accumulate from one year to the

---

<sup>4</sup> By definition, the period of damped oscillations induced by the autonomous equations is independent of  $\varepsilon_B$  – hence the vertical stripes of color in Figure 10.

<sup>5</sup> The analogy is not exact. In the wildfire model, sparks are generated not only by smoldering tinder, but also by lightning strikes and human activity. The epidemiological equivalent is the inflow of infectives into semi-isolated populations [76].

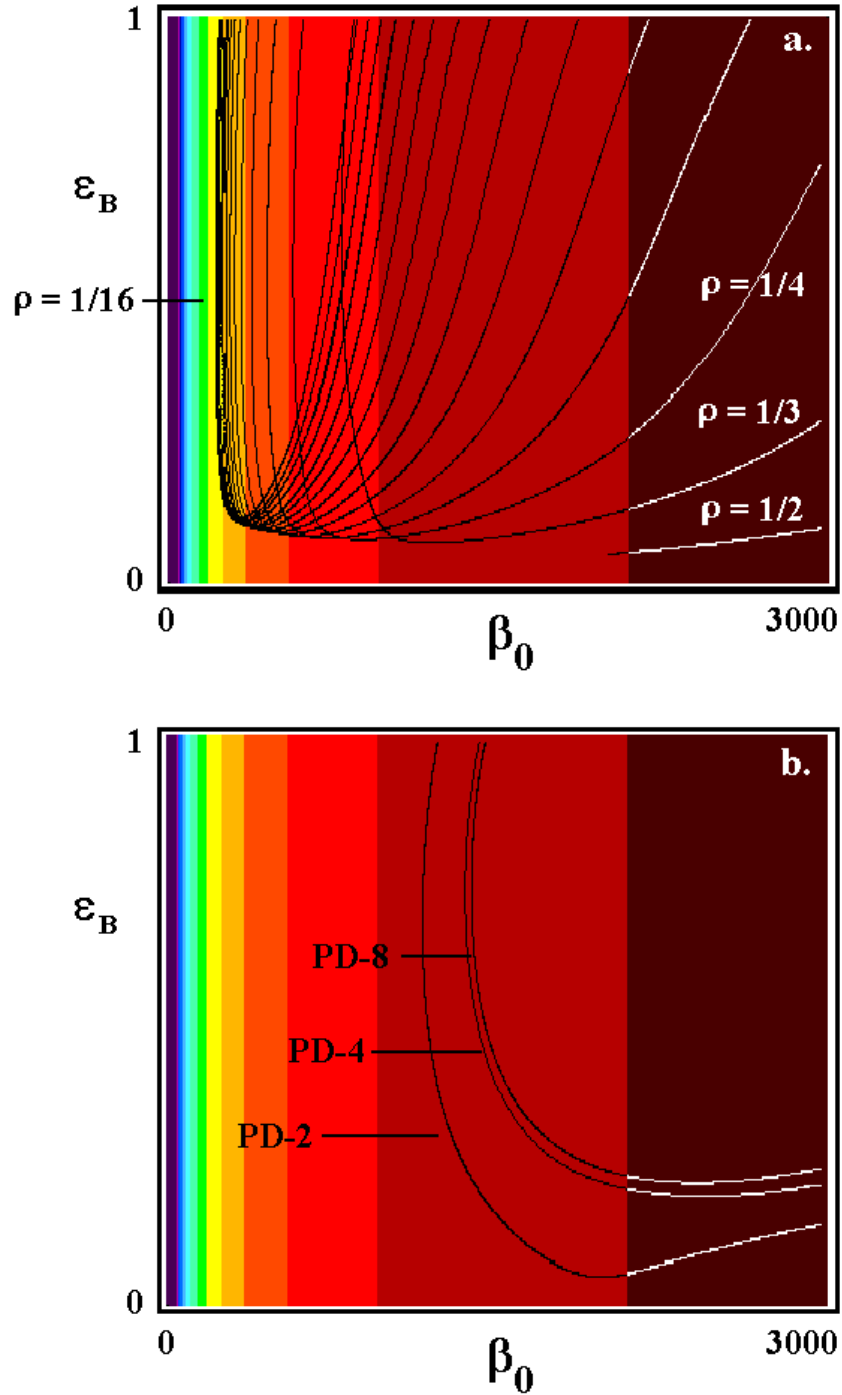


**Figure 10.** Autonomous vs. non-autonomous dynamics. The  $\rho = 1/2 - 1/16$  resonance horns (a.) and period-doubling curves (b.) are superposed on the  $\beta_0$ - $\varepsilon_B$  plane color-coded by the period,  $P$ , of damped oscillations about the endemic equilibrium,  $\mathbf{x}^*$ , of the autonomous equations. Color-coding is by the visible spectrum with dark red corresponding to  $P = 1$  y, and dark purple to  $P \geq 14$  y. Parameter values as in Figure 2.

next before being consumed more or less entirely in a major conflagration. Still further increases in combustibility return the system to the annual pattern – the tinder has become so flammable that it burns every summer and never accumulates. This explains the overall form of the control diagram.

To comprehend the consequences of varying non-contact related parameters, we observe that more tinder, *i.e.*, Susceptibles, results from increasing loss of immunity,  $r$ , and also from greater reproduction,  $m$ .<sup>6</sup> Likewise, decreasing latency (larger  $a$ ) increases the number of sparks. In both cases, transmission, which depends on  $S \times I$ , will be promoted, and bifurcation curves shifted left. Correspondingly, decreasing the infectious period (larger  $g$ ) impedes transmission (fewer sparks) and right-shifts the curves.

**Robustness.** Following [11, 15, 16, 23], we imagine that qualitative robustness of the  $\beta_0\text{-}\varepsilon_B$  control diagram likely explains the successful use [13] of historical data to parameterize equations that omit important biological details. If this is correct, age structure [5, 41], non-exponential transitions between host population classes [15, 16, 29], nonlinear transmission [73-75], more realistic forcing functions [11, 22, 41] and other complicating factors, will prove similar in their effect on overall parametric dependence to the results reported here.

The broader issue is the extent to which “bad” models can be made serviceable by judicious choice of parameter values. Ideally, one estimates parameters independently of experimental observations and compares observation to prediction. Failure to obtain satisfactory levels of correspondence is then deemed grounds for reformulating the model. But this presumes the ability to characterize accurately both the mechanisms and the parameters. As a rule, increased biological realism necessitates more equations and more parameters, with the consequent introduction of error. In short, the problem is analogous to what one encounters in the course of numerical integration: decreasing step size reduces the error per step, but there are more steps, so that the total error can increase

Alternatively, one can estimate some or all of the parameters from the data. This approach, utilized by Cushing and his associates ([77] and references therein) in modeling flour beetle population dynamics, has been applied to childhood epidemics by [13]. Previously, similar procedures were implemented [20, 39, 40] as an alternative to estimating seasonality directly [78, 79]. In these investigations, deterministic and stochastic versions of Equations (3) were solved for  $\varepsilon_B$  values corresponding to different dynamical regimes and the correspondence, as quantified by dynamical invariants [80], with historical notifications assessed. Like the far cleaner *Tribolium* studies, these investigations viewed the differential equations as proxies for the “real” equations that determine dynamics in nature.

---

<sup>6</sup> In the case of  $m$ , the effect would be more pronounced if births and deaths were decoupled.

Moreover, the manifest artificiality [73-75] of quadratic transmission and trigonometric seasonality [22] led to the expectation that the “best” values of  $\varepsilon_B$  would probably differ from those estimated independently. Note the underlying presumption: that patterns of parametric dependence in the “real” equations and the proxies are qualitatively equivalent, or, as Schaffer and Olsen [39] observed back in 1989,

“... that the differential equations ... exhibit a range of dynamical possibilities that reasonably approximate what one can expect to observe in nature, *though not necessarily for the same parameter values.*” [Emphasis added]

In short, one imagines that there exist points in parameter space for which the proxies reproduce what is actually going on – hence the importance of determining whether or not the observations reported here generalize.

**Conclusion.** We close on a dour note. Recurrent epidemics of childhood diseases and fluctuating densities of *Tribolium* in a bottle are sometimes held up as ecological equivalents of the inclined planes and frictionless pendula of classical mechanics. As such, they are presumed to be representative, at least in their essentials, of more complex real-world phenomena. But are they? In physics, one can point to whole disciplines, for example, celestial mechanics, in which simple equations so accurately predict nature, that theory and observation are effectively equivalent. Such is surely not the case in ecology where one substitutes potatoes for steel balls and hillsides for inclined planes, or, to put it another way, where multiple overlapping time and length scales are inescapable. Recalling the kingdom of the mapmakers [81], one can, of course, incorporate as much detail as desired *in simulo*, but only at the risk of repeating their folly while incurring the difficulties indicated above. How best to proceed, we believe, is the fundamental problem confronting theoretical ecology. Perhaps some combination of phenomenological equations, which admit to mathematical analysis, and detailed simulation will prove a recipe for progress – see, for example, Crommelin’s approach [82] to modeling the atmosphere.

### **Acknowledgements.**

We thank Aaron King who helped write the software. This study was supported by the Department of Ecology and Evolutionary Biology at the University of Arizona.

**References.**

- [1] Schaffer, W. M. and Bronnikova, T. V., 2007, Parametric dependence in model epidemics. *J. Biol. Dynam.*, (In press).
- [2] Anderson, R. M. and May, R. M., 1979, Population biology of infectious diseases: I. *Nature*, **280**, 361-367.
- [3] Keymer, A., 1982, Tapeworm infections. Pp. 109-138. **In**, Anderson, R. M. (Ed.) *Population Dynamics of Infectious Diseases: Theory and Applications*. (London: Chapman and Hall).
- [4] Anderson, R. M. and May, R. M., 1982, Directly transmitted infectious diseases: control by vaccination. *Science*, **215**, 451-454.
- [5] Bolker, B. M., 1993, Chaos and complexity in measles models. *IMA J. Math. Appl. Med. Biol.*, **10**, 83-95.
- [6] Blarer, A. and Dobelli, M., 1999, Resonance effects and outbreaks in ecological time series. *Ecol. Lett.*, **2**, 167-177.
- [7] Bolker, B. M. and Grenfell, B. T., 1993, Chaos and biological complexity in measles dynamics. *Proc. R. Soc. Lond. B*, **251**, 75-81.
- [8] Dietz, K., 1975, Transmission and control of arbovirus diseases. Pp. 104-121. **In**, Ludwig, D. and K. L. Cook (Eds.) *Epidemiology*. (Philadelphia: SIAM Press).
- [9] Dietz, K., 1976, The incidence of infectious diseases under the influence of seasonal perturbations. *Lect. Notes. Biomath.*, **11**, 1-15.
- [10] Drepper, F. R., Engbert, R. and Stollenwerk, N., 1994, Nonlinear time series analysis of empirical population dynamics. *Ecol. Modell.*, **75/76**, 171-181.
- [11] Earn, D. J. D., Rohani, P., Bolker, B. M. and Grenfell, B. T., 2000, A simple model for complex transitions in epidemics. *Science*, **287**, 667-670.
- [12] Engbert, R. and Drepper, F. R., 1994, Qualitative analysis of unpredictability: a case study from childhood epidemics. Pp. 204-215. **In**, Grasman, J. and G. van Straten (Eds.) *Predictability and Nonlinear Modelling in Natural Sciences and Economics*. (Dordrecht: Kluwer).
- [13] Keeling, M. J. and Grenfell, B. T., 2002, Understanding the persistence of measles: reconciling theory, simulation and observation. *Proc. R. Soc. London B.*, **269**, 335-343.
- [14] Kot, M., Schaffer, W. M., Truty, G. L., Graser, D. J. and Olsen, L. F., 1988, Changing criteria for order. *Ecol. Model.*, **43**, 75-110.

- [15] Lloyd, A. L., 2001a, Destabilization of epidemic models with the inclusion of realistic distributions of infectious periods. *Proc. R. Soc. Lond. B*, **268**, 985-993.
- [16] Lloyd, A. L., 2001b, Realistic distributions of infectious persistence in epidemic models: Changing patterns of persistence. *Theor. Pop. Biol.*, **60**, 59-71.
- [17] Lloyd, A. L. and Jansen, V. A., 2004, Spatiotemporal dynamics of epidemics: synchrony in metapopulation models. *Math. Biosci.*, **188**, 1-16.
- [18] Lloyd, A. L. and May, R. M., 1996, Spatial heterogeneity in epidemic models. *J. Theor. Biol.*, **179**, 1-11.
- [19] May, R. M. and Anderson, R. M., 1979, Population biology of infectious diseases: II. *Nature*, **280**, 455-461.
- [20] Olsen, L. F. and Schaffer, W. M., 1990, Chaos vs. noisy periodicity: Alternative hypotheses for childhood epidemics. *Science*, **249**, 499-504.
- [21] Olsen, L. F., Steinmetz, C. G., Tidd, C. W. and Schaffer, W. M., 1991. Childhood infections - Examples of chaos in the wild. Pp. 359-375, **In**, Moselkilde, E. and L. Moselkilde (eds.) *Complexity, Chaos and Biological Evolution*. (New York: Plenum Press).
- [22] Olsen, L. F., Truty, G. L. and Schaffer, W. M., 1988, A nonlinear dynamic study of six childhood diseases in Copenhagen, Denmark. *Theor. Pop. Biol.*, **33**, 344-380
- [23] Rohani, P., Keeling, M. J. and Grenfell, B. T., 2002, The interplay between determinism and stochasticity in childhood diseases. *Amer. Natur.*, **159**, 469-481.
- [24] Tidd, C. W., Olsen, L. F. and Schaffer, W. M., 1993. The case for chaos in childhood diseases. II. Predicting historical epidemics with mathematical models. *Proc. Biol. Sci. Roy. Soc. London*, **254**, 257-273.
- [25] Yorke, J. A., Nathanson, N., Piagiani, G. and Martin, J., 1979, Seasonality and the requirements for perpetuation and eradication of viruses in populations. *Am. J. Epidem.*, **109**, 103-123.
- [26] Aron, J. L. and Schwartz, I. B., 1984, Seasonality and period-doubling bifurcations in an epidemic model. *J. Theor. Biol.*, **110**, 665-679.
- [27] Billings, L. and Schwartz, I. B., 2002, Exciting chaos with noise: unexpected dynamics in epidemic outbreaks. *J. Math. Biol.*, **44**, 31-48.
- [28] Greeman, J., Kamo, M. and Boots, M., 2004, External forcing of ecological and epidemiological systems: a resonance approach. *Physica D*, **190**, 136-151.
- [29] Grossman, Z., 1980, Oscillatory dynamics in a model of infectious diseases. *Theor. Pop. Biol.*, **18**, 204-243.

- [30] Korobeinikov, A., 2004, Lyapunov functions and global properties for *SEIR* and *SEIS* epidemic models. *Math. Med. Biol.*, **21**, 75-83.
- [31] Kuznetsov, A. and Piccardi, C., 1994, Bifurcation analysis of periodic *SEIR* and *SIR* models. *J. Math. Biol.*, **32**, 109-121.
- [32] Li, G. and Zin, J., 2005, Global stability of an *SEI* epidemic model with general contact rate. *Chaos, Solitons and Fractals*, **23**, 997-1004.
- [33] Li, M. Y. and Muldowney, J. S., 1995, Global stability for the *SEIR* model in epidemiology. *Math. Biosci.*, **125**, 155-164.
- [34] Rand, D. H. and Wilson, H. B., 1991, Chaotic stochasticity: a ubiquitous source of unpredictability in epidemic models. *Proc. R. Soc. Lond. B*, **246**, 179-184.
- [35] Schaffer, W. M., 1985, Can nonlinear dynamics elucidate mechanisms in ecology and childhood epidemics? *IMA J. Math. Appl. Med. Biol.*, **2**, 221-252.
- [36] Schaffer, W. M., 1987, Chaos in ecology and epidemiology. Pp. 233-248. In, Holden, A. V., Degn, H. and L. F. Olsen (eds.) *Chaos in Biological Systems*. NATO Advanced Workshop. Chaos in Biology. (New York: Plenum Press).
- [37] Schaffer, W. M. and Kot, M., 1986a, Differential systems in ecology and epidemiology. Pp. 158-178. In, Holden, A. V. (ed.) *Chaos: An Introduction*. (Manchester: Univ. Manchester Press).
- [38] Schaffer, W. M. and Kot, M., 1986b, The coals that Newcastle forgot: Chaos in ecological systems. *Trends in Ecology and Evolution*, **1**, 58-63.
- [39] Schaffer, W. M. and Olsen, L. F., 1989, Chaos in childhood epidemics. Pp. 187-190. In, Abraham, N. B., Albano, A. M., Passamante, A. and P. E. Rapp. (eds.) *Measures of Complexity and Chaos*. Plenum Press. New York.
- [40] Schaffer, W. M., Olsen, L. F., Truty, G. L. and Fulmer, S. L., 1990, The case for chaos in childhood epidemics. Pp. 139-167. In, Krasner, S. (ed.), *The Ubiquity of Chaos*. (Washington, D.C.: AAAS Press).
- [41] Schenzle, D., 1984, An age-structured model of pre- and post-vaccination measles transmission. *IMA J. Math. Appl. Med. Biol.*, **1**, 169-191.
- [42] Schwartz, I. B., 1992, Small amplitude, long period outbreaks in seasonally driven epidemic models. *J. Math. Biol.*, **30**, 473-491.
- [43] Schwartz, I. B. and Smith, H. L., 1983, Infinite subharmonic bifurcations in an *SEIR* epidemic model. *J. Math. Biol.*, **18**, 233-253.

- [44] Fine, P. E. M. and Clarkson, J. A., 1982, Measles in England and Wales. I: An analysis of factors underlying seasonal patterns. *Int. J. Epidemiol.*, **11**, 5-14.
- [45] Khibnik, A. I., Kuznetsov, Y. A., Levitan, V. V. and Nikolaev, E. V., 1990-92, Interactive LOCAL BIFurcation Analyzer. Unpublished Manual to LOCBIF Version 2.
- [46] Kuznetsov, Y. A., 1995, *Elements of Applied Bifurcation theory*. (New York: Springer-Verlag).
- [47] Anderson, R. M., 1982, Directly transmitted viral and bacterial infections in man. Pp. 1-37. In: Anderson, R. M. (ed.) *Population Dynamics of Infectious Diseases: Theory and Applications*. (London: Chapman and Hall).
- [48] Hethcote, H. W., 2000, The mathematics of infectious diseases. *SIAM Review*. **42**, 599-653.
- [49] Lajmanovich, A. and Yorke, J. A., 1976, A deterministic model for gonorrhea in a nonhomogenous population. *Math. Biosci.*, **28**, 221-236.
- [50] Li, M. Y., Muldowny, J. S. and van den Driessche, P., 1995, Global stability of *SEIRS* models in epidemiology. *Math. Biosci.*, **125**, 1550164.
- [51] Hethcote, H. W., Stech, H. W. and van den Driessche, P., 1981, Nonlinear oscillations in epidemic models. *SIAM J. Appl. Math.*, **40**, 1-9.
- [52] Thompson, J. M. T. and Stewart, H. B., 2002, *Nonlinear Dynamics and Chaos* (West Sussex: John Wiley and Sons).
- [53] Arnol'd, V. I. 1983, *Geometrical Methods in the Theory of Ordinary Differential Equations*. (New York: Springer-Verlag).
- [54] King, A. A. and Schaffer, W. M. 1999. The rainbow bridge: Hamiltonian limits and resonance in predator-prey dynamics. *J. Math. Biol.*, **39**, 439-469.
- [55] Ott, E., 1993, *Chaos in Dynamical Systems* (Cambridge: Cambridge Univ. Press).
- [56] Grebogi, C., Ott, E. and Yorke, J. A., 1983, Crises, sudden changes in chaotic attractors and transient chaos. *Physica D.*, **7**, 181-200.
- [57] Schaffer, W. M., Kendall, B. E., Tidd, C. W. and Olsen, L. F., 1993, Transient periodicity and episodic predictability in biological dynamics. *IMA J. Math. Appl. Med. Biol.*, **10**, 217-247.
- [58] Vance, W. N. and Ross, J., 1991. Bifurcation structures of periodically forced oscillators. *Chaos*, **1**, 445-453.

- [59] Jackson, E. A., 1985, *Perspectives of Nonlinear Dynamics*. (Cambridge: Cambridge Univ. Press).
- [60] Roudferfer, V., Becker, N. G. and Hethcote, H. W., 1993, Waning immunity and its effect on vaccination schedules. *Math. Biosci.*, **124**, 59-82.
- [61] Zinkernagel, R. M., 2003, On natural and artificial vaccinations. *Ann. Rev. Immunol.*, **21**, 515-546.
- [62] Chen, F. P. and Chu, K. K., 1993. Subclinical rubella reinfection in pregnancy: report of a case. *J. Formos. Med. Assoc.*, **92**, 294-295.
- [63] Thompson, W. S., 1929, Population. *Amer. J. Sociol.*, **35**, 959-975.
- [64] Egerö, B., 2003, Global Disorder: An Important Agenda for 21st Century Population Studies. *Population Review*, **42**, 1-13.
- [65] London, W. A. and Yorke, J. A., 1973, Recurrent outbreaks of measles, chickenpox and mumps. I: Seasonal variation in contact rates. *Amer. J. Epidem.*, **98**, 453-468.
- [66] Glass, K., Xia, Y. and Grenfell, B. T., 2003, Interpreting time-series for continuous-time models – measles as a case study. *J. Theoret. Biol.*, **223**, 19-25.
- [67] Guckenheimer, J. and Holmes, P., 1983, *Nonlinear Oscillations, Dynamical Systems and Bifurcations of Vector Fields*. (New York: Springer-Verlag).
- [68] Devaney, R. L., 1986, *An Introduction to Chaotic Dynamical Systems*. (Menlo Park: Benjamin/Cummings).
- [69] Fed'kina, V. R., Bronnikova, T. V., and Ataulakhanov, F. I., 1984, Computer simulation of sustained oscillations in peroxidase-oxidase reaction. *Biophys. Chem.*, **19**, 259-264.
- [70] Fed'kina, V. R., Bronnikova, T. V. and Ataulakhanov, F. I., 1992, Phase space structure for peroxidase-oxidase reaction. *Biofizika*, **37**, 781-789 (Russian).
- [71] Fed'kina, V. R., Ataulakhanov, F. I. and Bronnikova, T. V., 1988, Forced regimes in peroxidase-oxidase reaction. *Theor. Exptl. Chem.*, **24**, 172-178 (Russian).
- [72] Schaffer, W. M., S. Ellner and Kot, M., 1986, Effects of noise on some dynamical models in ecology and epidemiology. *J. Math. Biol.*, **24**, 479-523.
- [73] Liu, W. M., Hethcote, H. W. and Levin, S. A., 1987, Dynamical behavior of epidemiological models with non-linear incidence rate. *J. Math. Biol.*, **25**, 359-380.
- [74] Heesterbeek, J. A. P. and Metz, J. A. J., 1993, The saturating contact rate in marriage and epidemic models. *J. Math. Biol.*, **31**, 529-539.

- [75] Korobeinikov, A. and Maini, P. K., 2005, Non-linear incidence and stability of infectious disease models. *Math. Med. Biol.*, **22**, 113-128.
- [76] Cliff, A. D., Haggett, P., Ord, J. K. and Versey, G. R., 1981, *Spatial Diffusion*. (Cambridge: Cambridge University Press).
- [77] Cushing, J. M., Costantino, R. F., Dennis, B., Desharnais, R. A. and Henson, S., 2002, *Chaos in Ecology: Experimental Nonlinear Dynamics*. (San Diego: Academic Press).
- [78] London, W. P. and Yorke, J. A., 1973, Recurrent outbreaks of measles, chickenpox, and mumps. I. Seasonal variation in contact rates. *Amer. J. Epidemiol.*, **98**, 453-468.
- [79] Schwartz, I. B., 1989, Nonlinear dynamics of seasonally driven epidemic models. Pp. 201-204, **In**, Eisenfeld, J. and Levin, D. S. (eds.), *Biomedical Modeling and Simulation*. (Berlin: J. C. Baltzer, A. G.).
- [80] Parker, T. S. and Chua, L. O., 1989, *Practical Numerical Algorithms for Chaotic Systems* (New York: Springer-Verlag).
- [81] Borges, J. L., 1999. On exactitude in science. **In**, Hurley, A. (Trans.) *Collected Fictions*. Copyright (New Yoerk: Penguin).
- [82] Crommelin, D., 2002, Homoclinic dynamics: A scenario for atmospheric ultralow-frequency variability. *J. Atm. Sci.*, **59**, 1533-1549.